Appl. Phys. 6, 249—256 (1975)

Applied Physics

Positron Annihilation in Copper: A k-Space Analysis

D. G. Lock and *R. N. West*

School of Mathematics and Physics, University of East Anglia, Norwich NOR 88C, Norfolk, England

Received 12 August 1974/Accepted 1 October 1974

Abstract. A new approach to the analysis of positron-annihilation long-slit angular distributions which can provide a more direct reflection of Fermi surface profile has been described in a recent publication. The analysis involves the periodic superposition of angular distributions which has the effect of converting a momentum distribution into a distribution in reduced Bloch wave vectors $\boldsymbol{k}$. When applied to data for a Cu crystal, having the resolved momentum component parallel to the [110] direction, the analysis results in excellent agreement with the computed surface of Halse and also provides a guide to the form and intensity of the angular distribution for core electron annihilation.

A similar treatment of the results for a [100] orientation, at first sight, appears less encouraging. However, a more careful appraisal supports the general value of the approach, the validity of the analysis for the [110] crystal orientation, and gives further clues to the form and anisotropy of the core distributions for Cu single crystals.

Index Headings: Positron — Copper

The results of positron annihilation studies of electronic structure in metals [1, 2] are frequently compared with those obtained from low temperature dHvA and magneto-accoustic investigations [3]. Inevitably, such comparisons are complicated by the fact that the low-temperature techniques reflect the occupancy of reduced Bloch wave vectors $\boldsymbol{k}$, whereas the most common long and short slit angular correlation measurements provide a detail obscuring integration of a positron-electron pair momentum distribution. The point detector geometry [4] can provide a more detailed probe of this momentum distribution but does not necessarily aid comparative analysis when complementary theory and experiment is invariably directed towards the prediction or measurement of Fermi surface parameters.

In a recent publication [5], henceforth referred to as LCW, we described a new approach to the analysis of long-slit angular distributions which may provide a better reflection of Fermi surface topology. When applied to our data for a Cu single crystal with (110) planes perpendicular to the resolved momentum component P_z, the analysis gave encouraging results. In this paper we present further results for Cu which allow more detailed consideration of both the strengths and weaknesses of the approach.

1. A Periodic Angular Distribution

The conventional long-slit angular distribution [2]

$$N(\theta)\,d\theta \equiv N(p_z)\,dp_z = A \int_{-\infty}^{+\infty}\int_{-\infty}^{+\infty} \varrho(\boldsymbol{p})\,dp_x dp_y \cdot dp_z\,, \tag{1}$$

where A is an arbitrary normalization constant and $\varrho(\boldsymbol{p})\,d^3\boldsymbol{p}$ is the electron-positron pair momentum

distribution. $p_z(\mathrm{AU}) = 137\,\theta$ where θ is the angle between the annihilation photon detectors. The analysis described in LCW is based on the construction of the distribution

$$F(p_z)\,dp_z = \sum_{P_z} N(p_z + P_z)\,dp_z\,,$$

where the P_z are the intersections of the p_z-axis with perpendicular planes of the appropriate reciprocal lattice set up in $\boldsymbol{p}$-space.

$F(p_z)$ possesses several desirable properties which are most clearly exposed if the positron and occupied electron states are represented, in the independent particle approximation, by Fourier series in reciprocal lattice vectors, $\boldsymbol{K}$, $\boldsymbol{G}$, i.e.

$$\begin{aligned} \psi_+(\boldsymbol{r}) &= \sum_{\boldsymbol{K}} A_{\boldsymbol{K}} \exp(i\boldsymbol{K}\cdot\boldsymbol{r}) \\ \psi_{\boldsymbol{k}}^n(\boldsymbol{r}) &= \sum_{\boldsymbol{G}} B_n(\boldsymbol{k}+\boldsymbol{G}) \exp[i(\boldsymbol{k}+\boldsymbol{G})\cdot\boldsymbol{r}]\,. \end{aligned} \tag{2}$$

Here n is a band index, and $\boldsymbol{k}$ is the reduced Bloch wave vector. Then, as shown in LCW, $F(p_z)$ assumes the form

$$\begin{aligned} F(p_z) = \mathrm{const} \sum_{\boldsymbol{P}} \iint_{PZ_2} dp_x dp_y \sum_{\mathrm{occ}\,\boldsymbol{k},n} \\ \cdot\,\delta(\boldsymbol{p}+\boldsymbol{P}-\boldsymbol{k}) \sum_{\boldsymbol{G}} |C_n(\boldsymbol{k}+\boldsymbol{G})|^2\,, \end{aligned} \tag{3}$$

where

$$C_n(\boldsymbol{k}+\boldsymbol{G}) = \sum_{\boldsymbol{K}} A_{\boldsymbol{K}} B_n(\boldsymbol{k}+\boldsymbol{G}-\boldsymbol{K})\,. \tag{4}$$

Equation (3) is derived from a superficially similar equation for $N(p_z)$ but is different in several important respects. The integration over all p_x, p_y in (1) here is replaced by a restricted integration over an appropriate zone, PZ_2, in the plane of reciprocal lattice points $\boldsymbol{P}$ at P_z, together with a sum over all the $\boldsymbol{P}$. As a consequence, contributions to $F(p_z)$ from different terms in the further sum over reciprocal lattice vectors $\boldsymbol{G}$ are superimposed unlike the corresponding contributions to $N(p_z)$ which may be spatially separated.

The importance of this superposition is most apparent if we consider the approximation of a plane wave (constant) positron wavefunction normalized to unity within a unit cell Ω. Then

$$\begin{aligned} &C_n(\boldsymbol{k}+\boldsymbol{G}) = \Omega^{-\frac{1}{2}} B_n(\boldsymbol{k}+\boldsymbol{G}) \\ &\text{and} \quad \sum_{\boldsymbol{G}} |C_n(\boldsymbol{k}+\boldsymbol{G})|^2 = \Omega^{-2} \end{aligned} \tag{5}$$

which thus provides a simple additional momentum independent factor which may readily be absorbed into that already present in (3). The contribution to $F(p_z)$ from all the states in the filled Brillouin zones is now of constant amplitude and cannot contribute to any structure in $F(p_z)$. The contribution from unfilled zones is simply proportional to the cross sectional areas of those parts of the Fermi surface, in a repeated zone scheme, which lie within the prism created by sweeping PZ_2 through all p_z and thus provides a measure of the Fermi surface topology.

In a real problem both these idealized results will be modified by the presence of higher momentum components (HMC) in the positron wavefunction and by additional momentum dependences caused by the electron-positron force. Nevertheless, as we shall attempt to demonstrate in subsequent sections, the resulting distortion of the Fermi surface images should be much less than that in the original $N(p_z)$ distribution.

2. Experimental, Results and Approximate Analysis

We have now applied the analysis suggested by Section 1 to angular correlation results for two ([110], [100]) orientations of a Cu single crystal. [111] and other orientations of lower symmetry are of limited value insofar as they involve a progressive reduction in the repeat distance p_z and increase in the area of the two-dimensional zone, PZ_2 [Eq. (3) and Figs. 2,

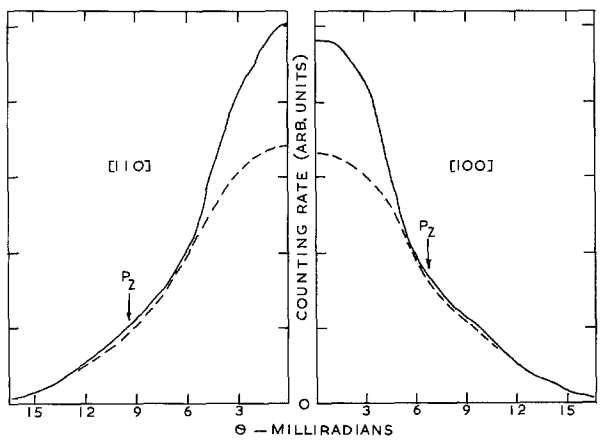

Fig. 1. Long slit angular distributions for [110] and [100] orientations of Cu single crystal. Each distribution has been folded about its centroid and, for the sake of clarity, a solid curve has been drawn through the individual 140 data points. The associated error bars are too small ($\pm 0.4\%$ at peak) for adequate presentation. The broken curves depict the limits of the contributions ascribed to annihilation from electron states in full Brillouin zones

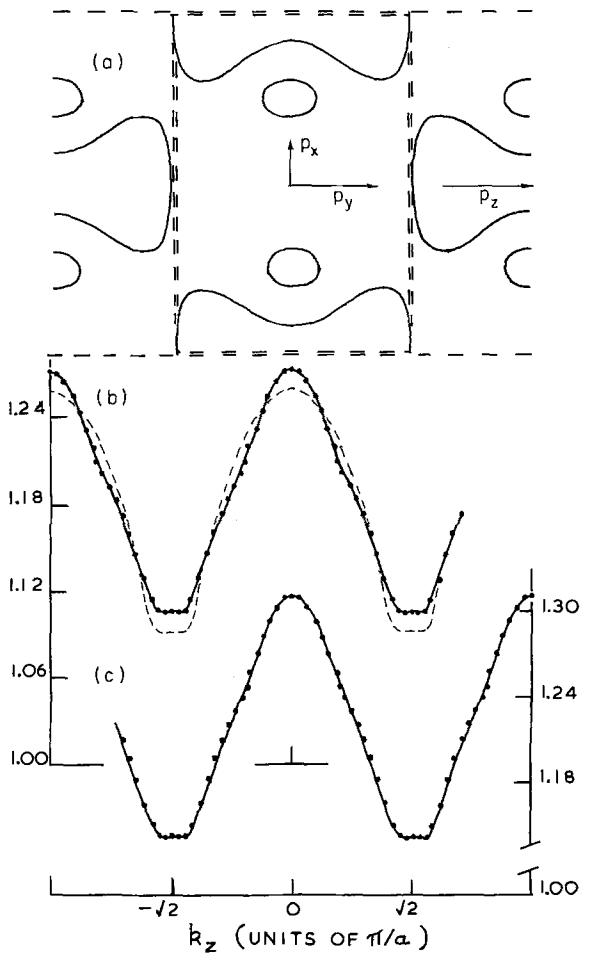

Fig. 2a—c. Fermi surface cross-sectional area profiles perpendicular to the [110] direction. (a) The volume of k-space involved in the measurements. The horizontal, broken lines represent the boundaries of a section parallel to the resolved momentum component and the double broken lines enclose the (perpendicular) region of integration PZ_2 [Eq. (3)], (b) Experimental profile (solid circles) compared with a spherical Fermi surface profile (broken curve) and the profile according to the Halse [6] representation (solid curve). (c) Same but with the Halse theoretical profile corrected for many electron enhancement effects [16]

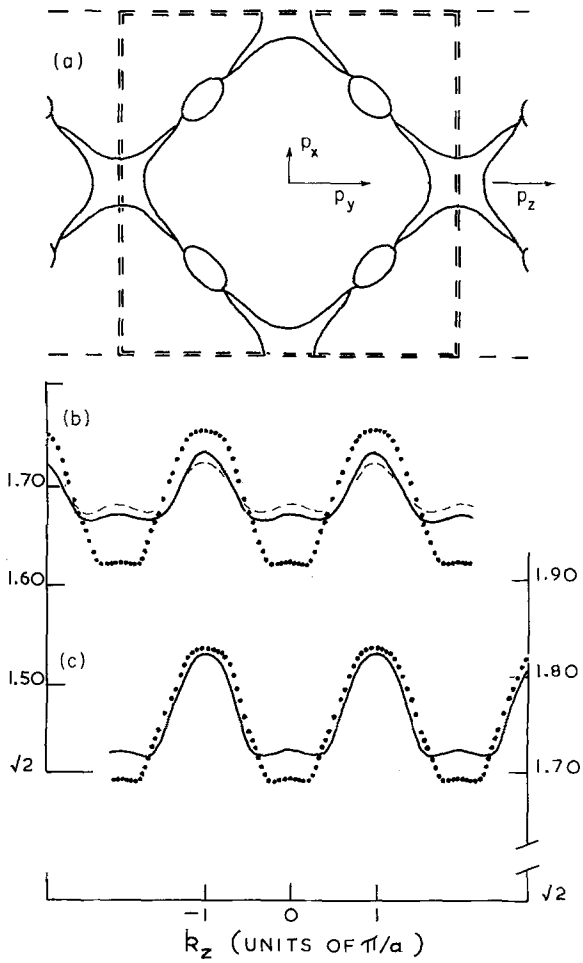

Fig. 3a–c. Fermi surface cross-sectional area profiles perpendicular to the [100] direction. The presentation is identical to that in Fig. 2.

3], which both suppresses the variations in $F(p_z)$ and severely complicates a subsequent analysis in terms of the Fermi surface shape.

The experimental procedures and treatment of the results were exactly, as described in LCW, and result in the long slit $N(p_z)$, and periodic $F(p_z)$, distributions shown, respectively, in Figs. 1, 2, and 3. As in LCW the $F(p_z)$ results are compared with theoretical Cu Fermi surface cross-sectional areas obtained from numerical integration of the Halse Cu 5 representation [6]. The theoretical curves (Figs. 2, 3) have been folded with the instrumental optical resolution function.

The experimental $F(p_z)$ for the [110] orientation, $F(110)$, shows variations in excellent agreement with the theoretical Fermi surface cross sections and a "best fit", based on the approximate, constant positron wavefunction theory of Section 1 provides a constant background filled Brillouin-zone contribution of partial area 0.84. A similar treatment of $F(100)$ is much less satisfactory. If, as is necessary, the partial core area is restrained to be as in $F(110)$ the observed variation in $F(100)$ is considerably larger than that predicted by the theoretical results. It is worth pointing out that no choice of constant amplitude core contribution can reproduce the observed variations in $F(100)$.

The excellent agreement between the approximate theory and experimental $F(110)$ seems too good to be entirely fortuitous. In the sections that follows we shall show that a belief in this result need not necessarily be compromised by the relatively poorer result for the [100] orientation.

3. Corrections to the Approximate Theory

3.1 Full Band Contributions

The approximate nature of the "sum rule" (5), $\Sigma_{\boldsymbol{G}}|C_n(\boldsymbol{k}+\boldsymbol{G})|^2=\Omega^{-2}$, was discussed in LCW with the aid of the simple tight binding approximation. An alternative but similar analysis, which has the virtue of being formally exact, is based on the Wannier functions [7],

$$a_n(\boldsymbol{r}-\boldsymbol{R}_i)=N^{-\frac{1}{2}}\sum_{\boldsymbol{k}}\psi_{\boldsymbol{k}}^n(\boldsymbol{r})\exp(-i\boldsymbol{k}\cdot\boldsymbol{R}_i) \tag{6}$$

centred about the N lattice sites $\boldsymbol{R}_i$ of the crystal. In this representation (cf. LCW)

$$\begin{aligned}\chi^n(\boldsymbol{k})&=\sum_{\boldsymbol{G}}|C_n(\boldsymbol{k}+\boldsymbol{G})|^2=\sum_{\boldsymbol{G}}\sum_{\boldsymbol{K}}\sum_{\boldsymbol{K}'}A_{\boldsymbol{K}}^*A_{\boldsymbol{K}'}\\&\quad\cdot B_n^*(\boldsymbol{k}+\boldsymbol{G}-\boldsymbol{K})\,B_n(\boldsymbol{k}+\boldsymbol{G}-\boldsymbol{K}')\\&=\Omega^{-1}\sum_{\boldsymbol{K}}\sum_{\boldsymbol{K}'}A_{\boldsymbol{K}}^*A_{\boldsymbol{K}'}\sum_{\boldsymbol{R}_i}\exp(i\boldsymbol{k}\cdot\boldsymbol{R}_i)\,S_{nn}(\boldsymbol{R}_i,\boldsymbol{K}-\boldsymbol{K}')\,.\end{aligned} \tag{7}$$

Here

$$S_{nn}(\boldsymbol{R}_i,\boldsymbol{K}-\boldsymbol{K}')=\int d^3\boldsymbol{r}\,a_n^*(\boldsymbol{r})a_n(\boldsymbol{r}-\boldsymbol{R}_i)\exp[i(\boldsymbol{K}-\boldsymbol{K}')\cdot\boldsymbol{r}] \tag{8}$$

are the matrix elements of $\exp[i(\boldsymbol{K}-\boldsymbol{K}')\cdot\boldsymbol{r}]$ with respect to the Wannier functions which, together with the additional factors in (7), provide coefficients for the Fourier expansion

$$\begin{aligned}\chi^n(\boldsymbol{k})=\sum_{rst}\chi_{rst}[&\cos(rak_x)\cos(sak_y)\cos(tak_z)\\&+\cos(rak_y)\cos(sak_z)\cos(tak_x)\\&+\cos(rak_z)\cos(sak_x)\cos(tak_y)]\,.\end{aligned} \tag{9}$$

Here a is the side of the f.c.c. cell and the sum over r, s, t, is restricted to those sets of indices which correspond to the $|\boldsymbol{R}_i|$ for that structure, i.e. (000), $(\frac{11}{22}0)$, (100), $(1\frac{11}{22})$, ... etc.

It is straightforward to integrate these functions over the appropriate PZ_2 so as to obtain some insight into the form of the possible variations in $F(p_z)$ for the full Brillouin zones. Thus, for p_z in the fundamental region, $-P_z<p_z<+P_z$, we find for a [100] orientation

$$\iint_{PZ_2}dp_x\,dp_y\,\chi^n(\boldsymbol{p})=\sum_r\chi_{roo}\cos(rak_z)\,.$$

The immediately apparent relationship between the indices of those terms in (9) which survive the integration and the indices defining the orientation is general. It indicates the relative independence of any consequent variations in the full Brillouin-zone contributions to the $F(p_z)$ for different orientations and thus the difficulty of any assessment of self-consistency between curves like those of Figs. 2 and 3. However, it also satisfies the primary aim of the present discussion, in that, the comparatively better agreement between the approximate theory and experimental data for $F(110)$ could easily arise from a fortuitous extinction of the dominant terms in (9) in the integration over PZ_2.

The relative importance of these various terms depends on both the positron and the electron momentum eigenfunctions. Calculations of the positron eigenfunctions in Cu exist [8, 9], and one can easily deduce from the data of Table 1 their effect in (7). For example,

$$\begin{aligned}\left[\sum_{\boldsymbol{K}}\sum_{\boldsymbol{K}'}A_{\boldsymbol{K}}^*A_{\boldsymbol{K}'}\right]_{(\boldsymbol{K}-\boldsymbol{K}'=\langle 220\rangle)}&\\\ll\left[\sum_{\boldsymbol{K}}\sum_{\boldsymbol{K}'}A_{\boldsymbol{K}}^*A_{\boldsymbol{K}}\right]_{(\boldsymbol{K}-\boldsymbol{K}'=\langle 200\rangle)}&\cdot\end{aligned} \tag{10}$$

The effect of such inequalities on the χ_{rst} of (9) is more obscure. In the light of the present results it is tempting to suggest, although we have been unable to show, that, in general, the most important (largest) $S_{nn}(\boldsymbol{R}_i,\boldsymbol{K}-\boldsymbol{K}')$ are those for which $\boldsymbol{K}-\boldsymbol{K}'$ and $\boldsymbol{R}_i$ are parallel. The Wannier functions are particularly useful for the derivation of algebraically exact results but are prohibitively difficult to calculate for other than the simplest non-degenerate bands [10]. For this reason we now make recourse to qualitative arguments in our discussion of the present results.

We would first point out the analogy between the $\chi^n(\boldsymbol{k})$ and the corresponding electron energy surfaces, $E_n(\boldsymbol{k})$, which can also be represented, via a Wannier function analysis, by a Fourier series, albeit with different coefficients [7]. The correspondence is certainly exact in the extreme tight-binding limit where there is no overlap between states on adjacent sites and both χ^n and E_n are $\boldsymbol{k}$-independent.

The energy band structure of Cu is well known [10], and can be regarded as consisting essentially of five narrow d bands and a broad nearly free electron band of $s-p$ character. The mixing or hybridization of the d states with the $s-p$ states is very important in many problems but the calculations of

Mijnarends [11] suggest that the effect of such hybridization on the total momentum distribution for all the occupied states is small. Thus it may not be too unrealistic to consider the probable contributions to $\chi^n(\boldsymbol{k})$ in the absence of hybridization. Then, the contributions to the $\boldsymbol{k}$-dependent terms in $\chi^n(\boldsymbol{k})$ from the narrow d bands could be expected to be much smaller than those from the broad $s-p$ band.

The argument can be equally well developed in Wannier function terms. Subject to the usual orthonormality condition [7], we have considerable freedom in the choice of the Wannier functions we use in (8). The most usual single band Wannier function, as defined in (6), may be considerably extended in space and give rise to many and large Fourier components in $E_n(\boldsymbol{k})$ and $\chi^n(\boldsymbol{k})$. However, appropriate selection of the basis states $\Psi_{\boldsymbol{k}}(\boldsymbol{r})$, from different bands can provide a much more localized Wannier function [7] corresponding to a smooth $E(\boldsymbol{k})$ and, we would argue, a small variation in $\chi(\boldsymbol{k})$. Thus we may well be able to confine the major variations in $\chi(\boldsymbol{k})$ to a single composite or pseudo band similar to the hybridization-free $s-p$ band of the preceding argument. Adopting this philosophy we now turn our attention to the $\chi(\boldsymbol{k})$ for such a band.

3.2 Nearly Free Electrons

A nearly free electron analysis based on suitably chosen model or pseudo-potential coefficients has been shown to be applicable to Fermi surface and other experimental noble metal data provided one is only concerned with states above the d bands. The major deviations from sphericity of the Cu Fermi surface along the [111] and [100] directions indicate the dominant role played by the $V(111)$ and $V(200)$ coefficients for which most of the available evidence suggests similar values $\sim 0.2\,Ry$ [12]. The nonlocality of this potential may well be severe but we shall now proceed with the assumption that the qualitative aspects of this picture apply throughout our pseudo band.

The electron energies and momentum eigenfunctions can, at least in principal, be obtained from the set of simultaneous equations [10]

$$[|\boldsymbol{k}+\boldsymbol{G}|^2 - E(\boldsymbol{k})]\, B(\boldsymbol{k}+\boldsymbol{G}) + \sum_{\boldsymbol{G}'} V_{\boldsymbol{G}-\boldsymbol{G}'}\, B(\boldsymbol{k}+\boldsymbol{G}') = 0\,. \tag{11}$$

In the case of a crystal having inversion symmetry the $V_{\boldsymbol{G}}$ and $B(\boldsymbol{k}+\boldsymbol{G})$ may be taken as real.

Over the major part of a nearly free electron band the $\Psi_{\boldsymbol{k}}(\boldsymbol{r})$ will be close to a single plane wave. Then $E \sim k^2$, $B(\boldsymbol{k}) \sim \Omega^{-\frac{1}{2}}$, and the remaining $B(\boldsymbol{k}+\boldsymbol{G})$ are small and we may readily deduce from (11) that

$$\Omega B(\boldsymbol{k}+\boldsymbol{G})\, B(\boldsymbol{k}) \simeq -\, V_{\boldsymbol{G}}(G^2 + 2\boldsymbol{k}\cdot\boldsymbol{G})^{-1}\,. \tag{12}$$

Such products will then provide the major contributions to the $\boldsymbol{k}$-dependence of $\chi(\boldsymbol{k})$ Eq. (7). The extent to which their effect will be felt in $F(p_z)$ following the double integration over PZ_2 may depend on the orientation. The strong dependence on $\boldsymbol{k}\cdot\boldsymbol{G}$ suggests a similar cancellation to that already noted in the Fourier series representation developed in Subsection 3.1. The establishment of a one to one correspondence between the formally exact cosine terms of (9) and the approximate expressions of (12) which have parallel planes of constant χ is impossible but a qualitative correlation is most plausible. Complete cancellation in a partially filled zone is also ruled out. However, in even a half filled zone the occupied states extend on average 0.8 of the way to the Brillouin zone boundary and some cancellation should always occur. These remarks, the inequality (10) of Sub-section 3.1, and the probability that $V(200) > V(220)$ together suggest that any HMC induced variations in $\chi(\boldsymbol{k})$ will be much more in evidence in $F(100)$ than $F(110)$.

The probable magnitude of the variations in $F(100)$ can best be assessed by consideration of states close to the $\langle 200\rangle$ square zone face. Here we can expect that all of the momentum eigenfunctions other than $B(\boldsymbol{k})$ and $B[\boldsymbol{k}+\boldsymbol{G}(200)]$ will be small. Again it can easily, be shown from (11) that

$$\Omega B(\boldsymbol{k}+\boldsymbol{G})\, B(\boldsymbol{k}) \simeq \pm\, V_{\boldsymbol{G}}[(G^2 + 2\boldsymbol{k}\cdot\boldsymbol{G})^2 + 4V_{\boldsymbol{G}}^2]^{-\frac{1}{2}} \tag{13}$$

for both the upper $(+)$ and lower $(-)$ bands. The sign is significant. The multiplying positron contributions are also negative and thus, for the lower band, the contribution to $\chi(\boldsymbol{k})$ is positive. The result is a consequence of the positive sign of $V(200)$ [12] and is also the case for $\boldsymbol{k} \sim \boldsymbol{G}(111)/2$, a fact overlooked in LCW. A calculation utilizing the positron data given in Table 1, and $V(200) \sim 0.2\ Ry$ [12] suggests, for a state at the Fermi surface with $\boldsymbol{k}$ along [100], an increase in $\chi(\boldsymbol{k})$, as compared to the value for a single plane wave, of the order of 4%, Table 1. The increase in $\chi(\boldsymbol{k})$ arising from the product

Table 1. Momentum eigenfunctions for the positron [9], A_G, and conduction electrons, $B(\boldsymbol{k}+\boldsymbol{G})$, in various approximations; Ω is the volume of the unit cell. The entries in the last column illustrate the probable effects of HMC in the total annihilation rate

$\boldsymbol{G}$	$\langle 000\rangle$	$\langle 111\rangle$	$\langle 200\rangle$	$\langle 220\rangle$	$\Omega^2 \sum_{\boldsymbol{G}} \lvert C_{\boldsymbol{G}}(\boldsymbol{k})\rvert^2$
$A_{\boldsymbol{G}}$ positron	0.1089	−0.0083	−0.0045	−0.0007	
$B(\boldsymbol{k}+\boldsymbol{G})$, free-electrons	0.1118	—	—	—	1.00
$B(\boldsymbol{k}+\boldsymbol{G})$, $\boldsymbol{k}=\boldsymbol{G}(111)/2$, electrons	0.0791	−0.0791	—	—	1.12
$B(\boldsymbol{k}+\boldsymbol{G})$, $\boldsymbol{k}=\boldsymbol{G}(200)/2$, electrons	0.0791	—	−0.0791	—	1.06
$B(\boldsymbol{k}+\boldsymbol{G})$, $k=k_F$; $\boldsymbol{k}\parallel\boldsymbol{G}(200)$, electrons	0.1054	—	−0.037	—	1.04

$B[\boldsymbol{k}+\boldsymbol{G}(111)]\,B(\boldsymbol{k})$ is somewhat larger (Table 1) but, as was earlier suggested, is likely to be much less in evidence in either $F(110)$ or $F(100)$ as a result of the integration over PZ_2.

In summary, we would suggest that variations in $\chi(\boldsymbol{k})$ arising from HMC should be most in evidence, if at all, in $F(100)$, but even there, as we shall see in the following section, they may be obscured by severer effects.

3.3 Electron Positron Correlations

Thus far our discussion has been formulated entirely within the confines of the independent particle approximation. The interacting electron-positron many particle aspect of the annihilation problem is most important in the calculation of positron lifetimes in metals but the momentum dependence of the annihilation rate predicted by the interacting electron gas theories, although significant, results in a relatively minor modification to the doubly integrated long-slit angular distribution [2]. The predicted slight swelling of the characteristic parabolic conduction electron distribution has been well established in the angular distributions of the alkali metals [13]. It also provides a beneficial ingredient in the theoretical analysis of results for some less simple metals [9].

Generalizations of the electron gas theories which attempt to take account of the HMC and other energy band aspects of electron behaviour in real metals have been developed. Hede and Carbotte [14] considered annihilation in a nearly free electron band and deduced electron gas like, k/k_F dependent enhancement factors which are common to all the momentum components in each participating electron state. Calculations of the enhancement factors for more tightly bound electrons [15] suggest little or no momentum dependence. The general conclusion to be drawn from these various analyses is that many electron enhancement effects will be similar for all the momentum components of each electron state and appreciable $\boldsymbol{k}$-dependence will be confined to wave vectors close to the Fermi surface. This preservation of HMC weightings is clearly of value in view of the construction (3) of $F(p_z)$.

The electron gas calculations of Kahana [16] provide enhancement factors that may be conveniently represented by the equation

$$\varepsilon(k) = a + b(k/k_F)^2 + c(k/k_F)^4 .$$

The constants a, b, and c are functions of electron gas density and the values, obtained by interpolation of the Kahana data, appropriate to the electron density corresponding to one electron per atom in Cu provide relative enhancements of 1.00 at $k=0$, 1.06 at $k=k_F/2$, and 1.37 at $k=k_F$. This relative increase in the probability of annihilation for states close to the Fermi surface is several times larger than that deduced in Subsection 3.2 as the probable result of HMC. However, we should point out that the considerably greater density of polarizable electron states in Cu, as compared with that defined by the free electron k_F, could result in a somewhat different k-dependence. Other more sophisticated considerations of interband transition [17] and nonspherical Fermi surface [18] enhancement effects suggest additional enhancement for those states in or around the $\langle 111\rangle$ zone face necks. However, a quantitative assessment of these effects is rather more difficult and qualitative consideration will be deferred to the following subsection.

3.4 Discussion

Of the various corrections to the approximate theory implied by the discussions of the preceding sections, the best defined is that arising from the Kahana [16] enhancement factor. Accordingly, we have applied a correction to the theoretical profiles. The enhancement factors were deduced in the manner

outlined in Subsection 3.3. The consequent modification to a spherical Fermi surface cross-section profile was expressed in the form of a factor $[1+\eta(p_z)]$ which was then applied to the Halse [6] cross-section profile. The corrected profile for each orientation was thereafter folded with a gaussian curve of width appropriate to the combined effects of the optical resolution and the additional smearing effect [2] of finite positron temperature. The positron effective mass [2] was taken to be the free electron mass.

The resulting "best fits" are shown in Figs. 2b and 3b. The goodness of the fit for $F(110)$ is hardly changed from that for the approximate theory except that the fractional area of the core contribution, assumed as before to be of the constant amplitude predicted by the approximate theory, is reduced from 0.84 to 0.81. A compatible fit (with the same core fraction) to $F(100)$ shows considerable improvement but some discrepancy remains.

Further quantitative corrections to the theoretical curves would require an explicit band structure study but a qualitative discussion is of some value. The theoretical $F(100)$ profile for a spherical Fermi surface is very similar to that for the Halse [6] surface (Fig. 3a) and thus any plausible change in the latter could hardly explain the experimental results. The HMC effects discussed in Subsection 3.2 also provide little scope for improving the fit since the effects are probably small (Table 1) and the prediction of an increase in $\chi(\boldsymbol{k})$ as the $\langle 200\rangle$ faces are approached is in opposite sense to that required. A very large additional many-body enhancement for states in the necks at the $\langle 111\rangle$ zone faces [17, 18] could provide for a beneficial correction to $F(100)$ but only at the expense of the fit for $F(110)$. A third, and in the view of the present authors, a more plausible cause of the bulk of the error in $F(100)$ is a small ($\sim 3\%$) variation in the large contribution from the full Brillouin zones.

In LCW we described an unfolding procedure which allows one to argue the form of the filled Brillouin zone contributions to $N(p_z)$ from the corresponding part of $F(p_z)$. If we assume that the residual discrepancies in $F(100)$ arise solely from the filled Brillouin zones, application of the unfolding procedure results in the broken curves of Fig. 1. The indicated "core" [5] anisotropy is then similar to that deduced in both previous calculations [11] and point detector [4, 19] measurements and, it should be noted, if correct, a consequence of positron wave-function HMC alone [19]. The consequent association of 81% of the total annihilation rate with the electron states in full Brillouin zones suggests many body enhancement factors comparable to those for the partly filled zone and must cast some doubt on the validity of our naive application of the Kahana [16] electron gas factors. The attribution of some or even all of the residual discrepancies between experiment and theory for $F(100)$ to $\langle 111\rangle$ zone face enhancement effects would imply a slightly smaller ($\sim 75\%$) "core" contribution but the qualitative picture would remain.

4. Conclusions

The experimental results and discussion presented in this paper provide an interpretation of angular distributions for Cu single crystals which is consistent with that obtained from previous more conventional analyses [2] but less dependent upon the detailed form of the electron wavefunctions. The agreement between the experimental and many body enhancement corrected profiles for $F(110)$ is striking and, in view of the arguments presented in Subsections 3.1 and 3.2, its significance need not be weakened by the relatively poorer result for $F(100)$. The residual discrepancies in $F(100)$ may, most reasonably, be attributed to a small positron HMC induced anisotropy in the large ($\sim 80\%$) contribution from full Brillouin zones.

The present application to a comparatively well understood system allows for a more general assessment of the value of the $F(p_z)$ superposition analysis. The method is only of value for systems and orientations in which the Fermi surface topology provides a significant variation in $F(p_z)$. The breakdown of the approximate theory brought about by positron HMC unfortunately precludes the potentially valuable precise identification of the contributions from full Brillouin zones. On the other hand, the complication of HMC is much less severe than that in the original angular distribution and even a semi-quantitative assessment of "core" contribution such as that described above is considerably better than that attainable without the super position procedure.

The superposition approach is likely to be of value in the analysis of angular distributions for alloys of Cu. The apparent cancellation of HMC and positron-electron correlation effects in $F(110)$, caused by the

p_x, p_y, integration in (3), presumably depends on the important symmetry aspects of the electron and positron band structure and should be preserved in dilute Cu alloys. Then, as we noted in [5], changes in Fermi surface topology should play the dominant role in consequent changes in $F(110)$. A paper is in preparation.

Acknowledgements. We should like to thank the Science Research Council, London, for financial support, Metals Research Ltd., Cambridge, who supplied the samples and the University of Manitoba for their hospitality to one of us (RNW) during the final stages of the preparation of this paper.

References

1. A. T. Stewart: In *Positron Annihilation*, ed. by A. T. Stewart L. O. Roellig (Academic Press, New York 1967) p. 17
2. R. N. West: Advanc. Phys. **22**, 263 (1973)
3. D. Schoenberg: In *The Physics of Metals*, Vol. 1, ed. by J. M. Ziman (C.U.P. Cambridge 1969) p. 62
4. D. Ll. Williams, E. H. Becker, P. Petjevich, G. Jones: Phys. Rev. Letters **20**, 448 (1968)
5. D. G. Lock, V. H. C. Crisp, R. N. West: J. Phys. F. (Metal Phys.) **3**, 561 (1973)
6. M. R. Halse: Phil. Trans. Roy. Soc. **265**, 507 (1969)
7. J. C. Slater: *Quantum Theory of Molecules and Solids* (McGraw-Hill, New York 1965) Vol. 2
8. S. Berko, J. S. Plaskett: Phys. Rev. **112**, 1877 (1958)
9. A. G. Gould, R. N. West, B. G. Hogg: Canad. J. Phys. **50**, 2294 (1972)
10. W. Jones, N. H. March: *Theoretical Solid State Physics* (Wiley, London 1973) Vol. 1
11. P. Mijnarends: Physica **63**, 235 (1973)
12. M. H. Cohen, V. Heine: In *Solid State Physics*, Vol. 24, ed. by F. Seitz, D. Turnbull (Gordon and Breech, New York 1970)
13. J. J. Donaghy, A. T. Stewart: Phys. Rev. **164**, 396 (1967)
14. B. B. J. Hede, J. P. Carbotte: J. Phys. Chem. Solids **33**, 727 (1962)
15. J. P. Carbotte, A. Salvadori: Phys. Rev. **162**, 290 (1967)
16. S. Kahana: Phys. Rev. **129**, 1622 (1963)
17. K. Fujiwara, T. Hyodo, J. Ohyama: J. Phys. Soc. Japan **33**, 1047 (1972)
18. K. Fujiwara, T. Hyodo: J. Phys. Soc. Japan **35**, 1664 (1973)
19. E. M. D. Senicki, E. H. Becker, A. G. Gould, B. G. Hogg: Phys. Letters **41** A, 293 (1972).